Tensor-Based Downlink Channel Reconstruction for FDD Massive MIMO

Lin Chen*, Xue Jiang*, Zhimeng Zhong†, Xingzhao Liu*, and Martin Haardt‡
*Department of Electronic Engineering, Shanghai Jiao Tong University, Shanghai, China
†Wireless Network RAN Research Department, Shanghai Huawei Technologies Co. LTD, Shanghai, China
‡Communications Research Laboratory, Ilmenau University of Technology, D-98684 Ilmenau, Germany

2021 55th Asilomar Conference on Signals, Systems, and Computers | 978-1-6654-5828-3/21/$31.00 ©2021 IEEE | DOI: 10.1109/IEEECONF53345.2021.9723411

***Abstract*—The acquisition of downlink channel state information (CSI) at the base station is a prerequisite for various applications in frequency division duplex (FDD) massive multiple-input multiple-output (MIMO) systems. To obtain accurate CSI, conventional approaches employ downlink training and feedback with a considerable overhead. In this paper, we exploit the partial reciprocity between FDD uplink and downlink channels to propose a tensor-based method for downlink channel reconstruction. According to this partial reciprocity, the tensor-based method efficiently estimates angle and delay parameters of the downlink channel from the uplink channel. Then, downlink training and feedback are incorporated by exploiting the sparse scattering property of the channel, so as to estimate the gain parameters of the multipath components with a small amount of overhead. Downlink channel reconstruction is achieved according to the estimated gain, angle and delay parameters. Experimental results on a Ray-tracing dataset demonstrate the effectiveness of the proposed downlink training and feedback scheme, and the superior channel estimation of the proposed tensor-based method compared with several alternative methods.**

***Index Terms*—Massive MIMO, FDD, channel estimation, tensor decomposition.**

I. Introduction

Frequency division duplex (FDD) is widely-used as a key duplexing mode in massive multiple-input multiple-output (MIMO) systems [1]–[9]. Massive MIMO deploys large-scale antenna arrays at the base station (BS) to ensure high spectral and energy efficiencies. However, due to the configuration of large-scale antenna arrays, it is challenging for FDD massive MIMO to acquire accurate downlink channel state information (CSI) at the BS [1]–[4].

In addition to the FDD mode, time division duplex (TDD) is another typical duplexing mode in MIMO systems [5]. In the TDD mode, the uplink and downlink channels satisfy the reciprocity property over the coherent transmission time. The channel reciprocity facilitates the estimation of downlink CSI, which can be obtained by the uplink pilot transmission from user equipments (UEs) [1], [2]. Although in the FDD mode, the full channel reciprocity is not accessible, partial channel characteristics are proved to be reciprocal, such as the angle and delay parameters of multipaths [1].

Based upon the partial reciprocity in the FDD mode, the uplink CSI can be exploited to estimate a part of the downlink CSI. In [5], the downlink channel is estimated according to the covariance matrix, which is induced from the uplink channel by virtue of angular reciprocity and power angular spectrum reciprocity. In [2], the angular reciprocity between the uplink and downlink channels is utilized for the downlink pilot design to reduce the training and feedback overhead. It also incorporates the angular domain channel sparsity and adopts the discrete Fourier transform (DFT) matrix as the dictionary to estimate the downlink CSI. However, in a real scenario, a propagation path may come from a random direction and not be exactly located on the DFT bins. The mismatch between propagation paths and DFT bins leads to the energy leakage effect, which degrades the *a priori* sparsity of the channel in the angular domain [6].

In [3], Han et al. reconstruct the FDD downlink channel by distinguishing different channel parameters discriminately. Frequency-dependent parameters are acquired from downlink training and feedback procedures. According to spatial reciprocity, frequency-independent parameters, i.e., angle and delay parameters, are entirely estimated from the uplink channel using the Newtonized orthogonal matching pursuit (NOMP) method [3], [10]. Since the parameter estimation in the uplink channel is significant for the downlink channel reconstruction, Garg et al. [7] modify the NOMP method to jointly estimate uplink parameters, so as to improve the downlink reconstruction performance. In [8], [9], superresolution and compressed sensing methods are proposed for angle and delay parameters estimation, which can be effectively used for FDD downlink channel reconstruction.

In this paper, we propose a tensor-based method for downlink channel reconstruction in FDD massive MIMO. Using the partial reciprocity between uplink and downlink channels, we estimate the angle and delay parameters of the dominant multipath components from the uplink channel. By representing the uplink channel as a multi-dimensional tensor, we employ the CANDECOMP/PARAFAC (CP) decomposition [11] for angle and delay estimation. After that, we devise an efficient downlink training and feedback scheme, from which to obtain the gain parameters of the multipath components in the downlink channel. Finally, the downlink channel is successfully reconstructed according to the estimated channel parameters.

Notation—Tensors, matrices, vectors, and scalars are represented by bold calligraphic ($\boldsymbol{\mathcal{X}}$), bold uppercase ($\mathbf{X}$), bold

This work is supported in part by the National Natural Science Foundation of China under Grant Grants 61971279 and 62022054, and in part by the Huawei Research Program 2021. *(Corresponding author: Xue Jiang.)*

lowercase ($\mathbf{x}$), and regular (x) letters, respectively. For a matrix $\mathbf{X} \in \mathbb{C}^{n_1 \times n_2}$, its ith column is written as $\mathbf{x}_i$, i.e., $\mathbf{X} = [\mathbf{x}_1, \cdots, \mathbf{x}_{n_2}]$. Superscripts $(\cdot)^T$, $(\cdot)^*$, $(\cdot)^H$, and $(\cdot)^\dagger$ denote the transpose, conjugate, Hermitian transpose, and pseudo-inverse, respectively. The symbols $\otimes$, $\odot$, $\circledast$, and $\circ$ stand for the Kronecker, Khatri-Rao, Hadamard, and outer products, respectively. We use $\angle$ to denote the phase angle of a complex number.

II. System Model

Consider a single-cell massive MIMO system, where the BS and the UE are equipped with M and 1 antennas, respectively. We focus on the FDD transmission mode using N subcarriers with spacing Δf. In the FDD mode, different carrier frequencies f^{ul} and f^{dl} are configured for uplink and downlink channels, respectively, whose response vectors with respect to the ith subcarrier can be expressed as

$$\begin{aligned} \mathbf{h}_i^{\text{ul}} &= \sum\nolimits_{l=1}^{L} \alpha_l^{\text{ul}} e^{-j2\pi(f^{\text{ul}}+(i-1)\Delta f)\tau_l} \mathbf{e}_l^{\text{ul}} \in \mathbb{C}^{M\times 1}, \\ \mathbf{h}_i^{\text{dl}} &= \sum\nolimits_{l=1}^{L} \alpha_l^{\text{dl}} e^{-j2\pi(f^{\text{dl}}+(i-1)\Delta f)\tau_l} \mathbf{e}_l^{\text{dl}} \in \mathbb{C}^{M\times 1}, \end{aligned} \tag{1}$$

where L represents the number of multipaths; α_l and τ_l are the complex gain and delay of the lth path, respectively; $\mathbf{e}_l^{\text{ul}}$ and $\mathbf{e}_l^{\text{dl}}$ are the uplink and downlink steering vectors of the BS antenna associated with the lth path, respectively.

It is worth mentioning that both $\mathbf{e}_l^{\text{ul}}$ and $\mathbf{e}_l^{\text{dl}}$ in (1) have different forms in terms of array configuration. Take $\mathbf{e}_l^{\text{ul}}$ as an example. For a uniform linear array (ULA), we have

$$\mathbf{e}_l^{\text{ul}}(\phi_l) = [1, e^{j\frac{2\pi}{\lambda^{\text{ul}}} d\sin(\phi_l)}, \cdots, e^{j\frac{2\pi}{\lambda^{\text{ul}}} d(M-1)\sin(\phi_l)}]^T, \tag{2}$$

where $\lambda^{\text{ul}} = c/f^{\text{ul}}$ denotes the wavelength with c being the speed of light; d represents the distance between adjacent antenna elements; ϕ_l denotes the direction of arrival of the lth path. As an alternative to a ULA, a uniform planar array (UPA) configuration, as illustrated in Fig. 1, yields

$$\mathbf{e}_l^{\text{ul}}(\theta_l, \varphi_l) = \mathbf{e}_{h,l}^{\text{ul}}(\theta_l, \varphi_l) \otimes \mathbf{e}_{v,l}^{\text{ul}}(\theta_l), \tag{3}$$

where θ_l and φ_l are the elevation and azimuth angles of the lth path, respectively. The antenna steering vectors in the horizontal and vertical directions are respectively expressed as

$$\begin{aligned} \mathbf{e}_{h,l}^{\text{ul}}(\theta_l,\varphi_l) &= [1, e^{j\frac{2\pi}{\lambda^{\text{ul}}} d_h \sin(\theta_l)\cos(\varphi_l)}, \ldots, e^{j\frac{2\pi}{\lambda^{\text{ul}}} d_h (M_h-1)\sin(\theta_l)\cos(\varphi_l)}]^T, \\ \mathbf{e}_{v,l}^{\text{ul}}(\theta_l) &= [1, e^{j\frac{2\pi}{\lambda^{\text{ul}}} d_v \cos(\theta_l)}, \ldots, e^{j\frac{2\pi}{\lambda^{\text{ul}}} d_v (M_v-1)\cos(\theta_l)}]^T, \end{aligned} \tag{4}$$

where M_h and M_v are the number of antennas in the horizontal and vertical directions, respectively, with $M = M_h \times M_v$.

Notice that the channel responses in (1) are based on a single subcarrier. When concatenating all subcarriers, we can obtain the response matrix for the uplink channel $\mathbf{H}^{\text{ul}} \in \mathbb{C}^{M\times N}$ as

$$\mathbf{H}^{\text{ul}} = [\mathbf{e}_1^{\text{ul}}, \cdots, \mathbf{e}_L^{\text{ul}}] \begin{bmatrix} \alpha_1^{\text{ul}} & & \\ & \ddots & \\ & & \alpha_L^{\text{ul}} \end{bmatrix} \begin{bmatrix} (\mathbf{f}_1^{\text{ul}})^T \\ \vdots \\ (\mathbf{f}_L^{\text{ul}})^T \end{bmatrix} = \mathbf{E}^{\text{ul}} \mathbf{\Lambda}^{\text{ul}} (\mathbf{F}^{\text{ul}})^T, \tag{5}$$

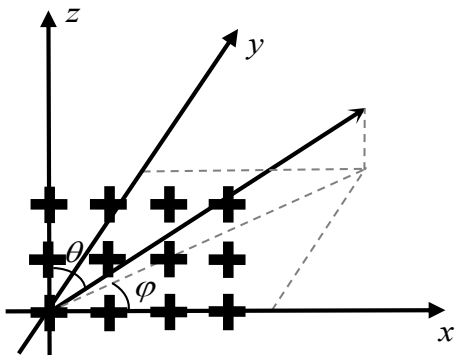

Fig. 1. Illustration of a UPA configuration. Each cross represents a pair of dual-polarized antennas.

where $\mathbf{f}_l^{\text{ul}} \in \mathbb{C}^{N\times 1} = [e^{-j2\pi f^{\text{ul}}\tau_l}, \cdots, e^{-j2\pi(f^{\text{ul}}+(N-1)\Delta f)\tau_l}]^T$. Of particular note is that (5) corresponds to the uplink channel response matrix in the case of an antenna array with a single polarization. However, a dual-polarized array shows a superior capacity and interference mitigation capability compared with the single-polarized version [12], [13]. Considering the dual-polarized MIMO uplink channel, four matrix blocks such as in (5) can be generated and integrated with identical $\mathbf{E}^{\text{ul}}$ and $\mathbf{F}^{\text{ul}}$, but different $\mathbf{\Lambda}^{\text{ul}}$ as

$$\mathbf{H}^{\text{ul}} = \begin{bmatrix} \mathbf{E}^{\text{ul}} \mathbf{\Lambda}_{(1,1)}^{\text{ul}} (\mathbf{F}^{\text{ul}})^T & \mathbf{E}^{\text{ul}} \mathbf{\Lambda}_{(1,2)}^{\text{ul}} (\mathbf{F}^{\text{ul}})^T \\ \mathbf{E}^{\text{ul}} \mathbf{\Lambda}_{(2,1)}^{\text{ul}} (\mathbf{F}^{\text{ul}})^T & \mathbf{E}^{\text{ul}} \mathbf{\Lambda}_{(2,2)}^{\text{ul}} (\mathbf{F}^{\text{ul}})^T \end{bmatrix} \in \mathbb{C}^{2M\times 2N}, \tag{6}$$

where $\mathbf{\Lambda}_{(p,q)}^{\text{ul}} \in \mathbb{C}^{L\times L}$ represents the gain matrix of the uplink channel when the polarization types of the receiver and the transmitter antennas are $p \in \{1,2\}$ and $q \in \{1,2\}$, respectively.

III. Tensor-based FDD Downlink Channel Reconstruction

In this section, we propose a tensor-based method to address the problem of FDD downlink channel reconstruction. We formulate the multi-dimensional FDD channel model, and employ the tensor decomposition for channel parameter estimation. By exploiting the partial reciprocity in the FDD mode, the angle and delay parameters of the downlink channel are estimated from the uplink channel, while the gain parameters are estimated from the proposed downlink training scheme. The process of downlink channel reconstruction is described in detail below.

A. Tensor-based Channel Representation

Beyond the conventional matrix modality, we rearrange the dual-polarization MIMO uplink channel in (6) into a multi-dimensional tensor modality. Here we distinguish two distinct array configurations at the BS. In the case of a ULA, we stack four matrix blocks in (6) along the third dimension to form a tensor $\boldsymbol{\mathcal{H}}^{\text{ul}} \in \mathbb{C}^{M\times N\times 4}$ such that

$$[\boldsymbol{\mathcal{H}}^{\text{ul}}]_{(p-1)\times 2+q} = \mathbf{E}^{\text{ul}} \mathbf{\Lambda}_{(p,q)}^{\text{ul}} (\mathbf{F}^{\text{ul}})^T, \tag{7}$$

where $[\boldsymbol{\mathcal{H}}^{\text{ul}}]_i$ denotes the ith frontal slice of $\boldsymbol{\mathcal{H}}^{\text{ul}}$. According to (7), $\boldsymbol{\mathcal{H}}^{\text{ul}}$ can be decomposed into the sum of L rank-one component tensors as

$$\boldsymbol{\mathcal{H}}^{\text{ul}} = \sum_{l=1}^{L} \mathbf{e}_l^{\text{ul}} \circ \mathbf{f}_l^{\text{ul}} \circ \mathbf{a}_l^{\text{ul}} = [\![\mathbf{E}^{\text{ul}}, \mathbf{F}^{\text{ul}}, \mathbf{A}^{\text{ul}}]\!], \tag{8}$$

where $[\![\ ]\!]$ denotes the Tucker operator [14], $\mathbf{e}_l^{\text{ul}}$ is defined in (2), and $\mathbf{a}_l^{\text{ul}} \in \mathbb{C}^{4\times 1}$ is the lth column of $\mathbf{A}^{\text{ul}} \in \mathbb{C}^{4\times L}$. In detail, $\mathbf{A}^{\text{ul}} = \left[\boldsymbol{\Lambda}_{(1,1)}^{\text{ul}}\mathbf{1}, \boldsymbol{\Lambda}_{(1,2)}^{\text{ul}}\mathbf{1}, \boldsymbol{\Lambda}_{(2,1)}^{\text{ul}}\mathbf{1}, \boldsymbol{\Lambda}_{(2,2)}^{\text{ul}}\mathbf{1}\right]^T$, where $\mathbf{1} \in \mathbb{R}^{L\times 1}$ is a vector with all entries being 1's.

In the case of a UPA, we incorporate (3) to refine the antenna steering matrix $\mathbf{E}^{\text{ul}}$ as the Khatri-Rao product of the horizontal direction matrix $\mathbf{E}_h^{\text{ul}}$ and the vertical direction matrix $\mathbf{E}_v^{\text{ul}}$, i.e., $\mathbf{E}^{\text{ul}} = \mathbf{E}_h^{\text{ul}} \odot \mathbf{E}_v^{\text{ul}}$. In this way, the three-dimensional tensor representation for the channel model in (8) is extended to a four-dimensional representation $\boldsymbol{\mathcal{H}}^{\text{ul}} \in \mathbb{C}^{M_h\times M_v\times N\times 4}$ as

$$\boldsymbol{\mathcal{H}}^{\text{ul}} = \sum_{l=1}^{L} \mathbf{e}_{h,l}^{\text{ul}} \circ \mathbf{e}_{v,l}^{\text{ul}} \circ \mathbf{f}_l^{\text{ul}} \circ \mathbf{a}_l^{\text{ul}} = [\![\mathbf{E}_h^{\text{ul}}, \mathbf{E}_v^{\text{ul}}, \mathbf{F}^{\text{ul}}, \mathbf{A}^{\text{ul}}]\!], \tag{9}$$

where $\mathbf{e}_{h,l}^{\text{ul}} \in \mathbb{C}^{M_h\times 1}$ and $\mathbf{e}_{v,l}^{\text{ul}} \in \mathbb{C}^{M_v\times 1}$ are defined in (4), and they are the lth column of $\mathbf{E}_h^{\text{ul}}$ and $\mathbf{E}_v^{\text{ul}}$, respectively.

B. Uplink Channel Parameters Estimation

Equations (8) and (9) lead to the CP decomposition [11] for the tensor of the uplink channel. Hence, the channel estimation problem from noise-corrupted measurements can be addressed by an approximate low-rank CP decomposition. Taking the UPA and Gaussian noise scenario as an example, it yields the following optimization problem:

$$\min_{\mathbf{E}_h^{\text{ul}}, \mathbf{E}_v^{\text{ul}}, \mathbf{F}^{\text{ul}}, \mathbf{A}^{\text{ul}}} \|\boldsymbol{\mathcal{H}}^{\text{ul}} - [\![\mathbf{E}_h^{\text{ul}}, \mathbf{E}_v^{\text{ul}}, \mathbf{F}^{\text{ul}}, \mathbf{A}^{\text{ul}}]\!]\|_F^2, \tag{10}$$

which can be efficiently solved by the alternating least-squares (ALS) method [11]. The ALS method identifies different optimization variables in an alternating iterative manner. With respect to the kth iteration, each optimization variable in (10) is updated in turn, resulting in the following system:

$$\begin{aligned}
(\mathbf{E}_h^{\text{ul}})_{k+1}^T &= \arg\min_{(\mathbf{E}_h^{\text{ul}})^T} \|\mathbf{H}_{(1)}^{\text{ul}} - ((\mathbf{E}_v^{\text{ul}})_k \odot \mathbf{F}_k^{\text{ul}} \odot \mathbf{A}_k^{\text{ul}})(\mathbf{E}_h^{\text{ul}})^T\|_F^2 \\
&= ((\mathbf{E}_v^{\text{ul}})_k \odot \mathbf{F}_k^{\text{ul}} \odot \mathbf{A}_k^{\text{ul}})^\dagger \mathbf{H}_{(1)}^{\text{ul}}, \\
(\mathbf{E}_v^{\text{ul}})_{k+1}^T &= \arg\min_{(\mathbf{E}_v^{\text{ul}})^T} \|\mathbf{H}_{(2)}^{\text{ul}} - (\mathbf{F}_k^{\text{ul}} \odot \mathbf{A}_k^{\text{ul}} \odot (\mathbf{E}_h^{\text{ul}})_{k+1})(\mathbf{E}_v^{\text{ul}})^T\|_F^2 \\
&= (\mathbf{F}_k^{\text{ul}} \odot \mathbf{A}_k^{\text{ul}} \odot (\mathbf{E}_h^{\text{ul}})_{k+1})^\dagger \mathbf{H}_{(2)}^{\text{ul}}, \\
(\mathbf{F}^{\text{ul}})_{k+1}^T &= \arg\min_{(\mathbf{F}^{\text{ul}})^T} \|\mathbf{H}_{(3)}^{\text{ul}} - (\mathbf{A}_k^{\text{ul}} \odot (\mathbf{E}_h^{\text{ul}})_{k+1} \odot (\mathbf{E}_v^{\text{ul}})_{k+1})(\mathbf{F}^{\text{ul}})^T\|_F^2 \\
&= (\mathbf{A}_k^{\text{ul}} \odot (\mathbf{E}_h^{\text{ul}})_{k+1} \odot (\mathbf{E}_v^{\text{ul}})_{k+1})^\dagger \mathbf{H}_{(3)}^{\text{ul}}, \\
(\mathbf{A}^{\text{ul}})_{k+1}^T &= \arg\min_{(\mathbf{A}^{\text{ul}})^T} \|\mathbf{H}_{(4)}^{\text{ul}} - ((\mathbf{E}_h^{\text{ul}})_{k+1} \odot (\mathbf{E}_v^{\text{ul}})_{k+1} \odot \mathbf{F}_{k+1}^{\text{ul}})(\mathbf{A}^{\text{ul}})^T\|_F^2 \\
&= ((\mathbf{E}_h^{\text{ul}})_{k+1} \odot (\mathbf{E}_v^{\text{ul}})_{k+1} \odot \mathbf{F}_{k+1}^{\text{ul}})^\dagger \mathbf{H}_{(4)}^{\text{ul}},
\end{aligned} \tag{11}$$

where $\mathbf{H}_{(i)}^{\text{ul}}$ denotes the i-mode unfolding of $\boldsymbol{\mathcal{H}}^{\text{ul}}$ [15], and the pseudo-inverse operator can be efficiently implemented using $(\mathbf{X}_1 \odot \mathbf{X}_2 \odot \mathbf{X}_3)^\dagger = (\mathbf{X}_1^H\mathbf{X}_1 \circledast (\mathbf{X}_2^H\mathbf{X}_2) \circledast (\mathbf{X}_3^H\mathbf{X}_3))^{-1}(\mathbf{X}_1 \odot \mathbf{X}_2 \odot \mathbf{X}_3)^H$ [11].

After obtaining four factor matrices $\hat{\mathbf{E}}_h^{\text{ul}}$, $\hat{\mathbf{E}}_v^{\text{ul}}$, $\hat{\mathbf{F}}^{\text{ul}}$, and $\hat{\mathbf{A}}^{\text{ul}}$ by the ALS method, we estimate the angle and delay parameters of the multipath components by exploiting the rotational invariant property [13] of $\hat{\mathbf{E}}_h^{\text{ul}}$, $\hat{\mathbf{E}}_v^{\text{ul}}$ and $\hat{\mathbf{F}}^{\text{ul}}$ as

$$\begin{cases}
\sin(\hat{\theta}_l)\cos(\hat{\varphi}_l) = \dfrac{\lambda^{\text{ul}} \cdot \angle\left((\overline{\mathbf{e}}_{h,l}^{\text{ul}})^H \underline{\mathbf{e}}_{h,l}^{\text{ul}}\right)}{2\pi d_h}, & (12) \\
\cos(\hat{\theta}_l) = \dfrac{\lambda^{\text{ul}} \cdot \angle\left((\overline{\mathbf{e}}_{v,l}^{\text{ul}})^H \underline{\mathbf{e}}_{v,l}^{\text{ul}}\right)}{2\pi d_v}, & (13) \\
\hat{\tau}_l = \dfrac{\angle\left((\overline{\mathbf{f}}_l^{\text{ul}})^H \underline{\mathbf{f}}_l^{\text{ul}}\right)}{-2\pi\Delta f}, & (14)
\end{cases}$$

where $\overline{\mathbf{f}}_l^{\text{ul}}$ and $\underline{\mathbf{f}}_l^{\text{ul}} \in \mathbb{C}^{(N-1)\times 1}$ are composed of the first and last $(N-1)$ entries of $\hat{\mathbf{f}}_l^{\text{ul}} \in \mathbb{C}^{N\times 1}$, respectively; $\overline{\mathbf{e}}_l^{\text{ul}}$ and $\underline{\mathbf{e}}_l^{\text{ul}}$ can be defined similarly. Note that (12) and (13) naturally hold based on the antenna array configuration of UPA, while (14) holds because the subcarrier spacing used in the FDD mode is fixed as Δf. Using (12)–(14) to estimate the channel parameters is computationally efficient, but may lead to suboptimal solutions [13]. Instead, sinusoidal parameter estimation methods, such as root-MUSIC [16] and principal-singular-vector utilization for modal analysis (PUMA) [17], can improve the estimation accuracy, but require higher computational complexities than using (12)–(14).

C. Downlink Training and Reconstruction

In the FDD mode, angle and delay parameters of the multipath components are frequency-independent, and can be estimated from the uplink channel used for the downlink channel reconstruction [1], [3], [4]. However, it is reported that the gain parameters of the multipath components are frequency-dependent [1], and thus need to be acquired through the downlink training and feedback. In the downlink training stage, the BS transmits the pilots over K successive OFDM symbols $\mathbf{S} \in \mathbb{C}^{M\times K}$. Suppose in each OFDM symbol, comb-type all-ones pilots are uniformly inserted into N_p of all N subcarriers [3]. Then, the received pilot signal under the configuration of a single-polarized antenna array is given by

$$\mathbf{Y} = \mathbf{H}^T\mathbf{S} + \mathbf{N}, \tag{15}$$

where $\mathbf{N} \in \mathbb{C}^{N_p\times K}$ denotes the noise matrix. $\mathbf{H} \in \mathbb{C}^{M\times N_p}$ is the subset of downlink channels occupied by N_p subcarriers as

$$\mathbf{H} = \left[\mathbf{e}_1^{\text{dl}}, \cdots, \mathbf{e}_L^{\text{dl}}\right] \begin{bmatrix} \alpha_1^{\text{dl}} & & \\ & \ddots & \\ & & \alpha_L^{\text{dl}} \end{bmatrix} \begin{bmatrix} \mathbf{f}_1^T \\ \vdots \\ \mathbf{f}_L^T \end{bmatrix} = \mathbf{E}^{\text{dl}}\boldsymbol{\Lambda}^{\text{dl}}\mathbf{F}^T, \tag{16}$$

where $\mathbf{f}_l \in \mathbb{C}^{N_p\times 1} = [e^{-j2\pi f^{\text{dl}}\tau_l}, e^{-j2\pi(f^{\text{dl}}+n\Delta f)\tau_l}, \cdots, e^{-j2\pi(f^{\text{dl}}+n(N_p-1)\Delta f)\tau_l}]^T$ under the condition $n = \lfloor N/N_p \rfloor$.

In the traditional pilot scheme, BS transmits the orthogonal pilots on different antenna elements with $K \geq M$, so that

the subset of downlink channel can be estimated by the least-squares method [2]

$$\hat{\mathbf{H}} = (\mathbf{S}^*\mathbf{S}^T)^{-1}\mathbf{S}^*\mathbf{Y}^T. \tag{17}$$

However, the requirement of $K \geq M$ is expensive for massive MIMO systems due to the large number of antennas at the BS. Fortunately, in the sparse multipath scenario, such as the millimeter wave channel [18], the downlink training overhead can be significantly reduced. By exploiting the sparse scattering nature of the channel, we can estimate angle, delay and gain parameters of the channel with a reduced number of paths such that $L \leq M$. To estimate the gain parameters, the downlink training model in (15) is combined with (16) and rewritten as

$$\mathbf{Y} = \mathbf{F}\mathbf{\Lambda}^{\text{dl}}(\mathbf{E}^{\text{dl}})^T\mathbf{S} + \mathbf{N}. \tag{18}$$

Extending (18) from the single-polarized to a dual-polarized antenna array, we consider the same pilot transmission for all polarization types, as suggested in [13], and then stack the received pilot signal to form a tensor $\boldsymbol{\mathcal{Y}} \in \mathbb{C}^{N_p \times K \times 4}$ as

$$[\boldsymbol{\mathcal{Y}}]_{(p-1)\times 2+q} = \mathbf{F}\mathbf{\Lambda}^{\text{dl}}_{(p,q)}(\mathbf{E}^{\text{dl}})^T\mathbf{S} + \mathbf{N}_{(p,q)}, \tag{19}$$

where $\mathbf{\Lambda}^{\text{dl}}_{(p,q)} \in \mathbb{C}^{L\times L}$ can be defined similarly as $\mathbf{\Lambda}^{\text{ul}}_{(p,q)}$ in (6) with $p, q \in \{1, 2\}$. Derived from (19), the CP decomposition for the tensor of received pilot symbols is expressed as

$$\boldsymbol{\mathcal{Y}} = [\![\mathbf{F}, \mathbf{S}^T\mathbf{E}^{\text{dl}}, \mathbf{A}^{\text{dl}}]\!] + \boldsymbol{\mathcal{N}}, \tag{20}$$

where the downlink gain parameter matrix $\mathbf{A}^{\text{dl}} \in \mathbb{C}^{4\times L}$ is defined in a similar fashion as $\mathbf{A}^{\text{ul}}$ in (8), and can be recovered by the least-squares method as

$$\begin{aligned}(\hat{\mathbf{A}}^{\text{dl}})^T &= (\mathbf{F} \odot (\mathbf{S}^T\mathbf{E}^{\text{dl}}))^{\dagger}\mathbf{Y}_{(3)} \\ &= [\mathbf{F}^H\mathbf{F} \circledast ((\mathbf{E}^{\text{dl}})^H\mathbf{S}^*\mathbf{S}^T\mathbf{E}^{\text{dl}})]^{-1}(\mathbf{F}\odot(\mathbf{S}^T\mathbf{E}^{\text{dl}}))^H\mathbf{Y}_{(3)}.\end{aligned} \tag{21}$$

It is obvious that the above recovery requires $\mathbf{F} \odot (\mathbf{S}^T\mathbf{E}^{\text{dl}})$ to be full column-rank, which implies that the required number of downlink pilots is $K \geq \lceil L/N_p \rceil$. Compared with traditional pilot transmission schemes, the proposed scheme in (21) can significantly reduce the downlink training overhead in the sparse multipath scenario.

After the downlink gain parameters are fed back to the BS, the BS combines them with the angle and delay parameters to reconstruct the downlink channel as

$$\hat{\boldsymbol{\mathcal{H}}}^{\text{dl}} = \sum_{l=1}^{L} \hat{\mathbf{e}}^{\text{dl}}_{h,l} \circ \hat{\mathbf{e}}^{\text{dl}}_{v,l} \circ \hat{\mathbf{f}}^{\text{dl}}_{l} \circ \hat{\mathbf{a}}^{\text{dl}}_{l} = [\![\hat{\mathbf{E}}^{\text{dl}}_{h}, \hat{\mathbf{E}}^{\text{dl}}_{v}, \hat{\mathbf{F}}^{\text{dl}}, \hat{\mathbf{A}}^{\text{dl}}]\!], \tag{22}$$

where $\hat{\mathbf{f}}^{\text{dl}}_{l} = [e^{-j2\pi f^{\text{dl}}\hat{\tau}_l}, e^{-j2\pi(f^{\text{dl}}+\Delta f)\hat{\tau}_l}, \cdots, e^{-j2\pi(f^{\text{dl}}+N\Delta f)\hat{\tau}_l}]$; $\hat{\mathbf{e}}^{\text{dl}}_{h,l}$ and $\hat{\mathbf{e}}^{\text{dl}}_{v,l}$ are constructed from the estimated angle parameters $\sin(\hat{\theta}_l)\cos(\hat{\varphi}_l)$ and $\cos(\hat{\theta}_l)$ as in (4), respectively.

IV. Experimental Results

We evaluate the performance of the proposed tensor-based method for FDD downlink channel reconstruction using a Ray-tracing dataset. Measurements of this dataset were conducted in the campus of Shanghai Jiao Tong University. At the BS, we use a UPA with the polarization. The number of antennas in horizontal and vertical directions is $M_h = 8$ and $M_v = 2$, respectively, while the UE is equipped with a single antenna. As shown in Fig. 2, UEs are treated as rectangular and placed at equal intervals within the blue sector served by the BS. The dataset consists of 11584 UEs, five of which are shown in Fig. 2. Each UE corresponds to an uplink channel and a downlink channel. The carrier frequencies of the uplink and downlink channels are 2.04GHz and 2.14GHz, respectively. A total of $N = 601$ subcarriers with the interval $[-300 : 1 : 300]\times$15kHz are used for channel generation.

To reconstruct the downlink channel for each UE scenario, we first estimate angle and delay parameters from the uplink channel in the presence of white Gaussian noise at SNR=15dB. In the above estimation, we adopt PUMA after ALS for the proposed tensor-based method. Then, the gain parameters of downlink channel are estimated using the traditional pilot training scheme in (17) with $N_p = N$ and $K = M$ at SNR=15dB. After that, the downlink channel is reconstructed by (22), and the reconstruction accuracy is measured by the widely-used normalized mean square error (NMSE) as

$$\text{NMSE} = \|\hat{\boldsymbol{\mathcal{H}}}^{\text{dl}} - \boldsymbol{\mathcal{H}}^{\text{dl}}\|_F^2 / \|\boldsymbol{\mathcal{H}}^{\text{dl}}\|_F^2, \tag{23}$$

where $\hat{\boldsymbol{\mathcal{H}}}^{\text{dl}}$ is the reconstruction result of the groundtruth $\boldsymbol{\mathcal{H}}^{\text{dl}} \in \mathbb{C}^{M_h\times M_v\times N\times 4}$.

Fig. 3 plots the cumulative distribution function (CDF) of the NMSE for all UEs' downlink channel reconstruction in the dataset. The proposed tensor-based method is compared with three alternative methods, including overcomplete DFT [6], compressed sensing [8] and superresolution [9]. Notice that the compressed sensing, superresolution and the proposed methods require a predefined number of paths L. In the Ray-tracing dataset, the number of paths ranges from dozens to hundreds and varies with different UE scenarios. Considering that the number of paths is unknown in advance, we uniformly set $L = 16$, which equals to the number of antennas at the BS, for these there methods in handling all UE scenarios. For the overcomplete DFT method, we also select 16 bases with the highest energies among all overcomplete DFT bases for channel reconstruction to ensure the fairness. Based upon the uplink and downlink reciprocity property, the locations of 16

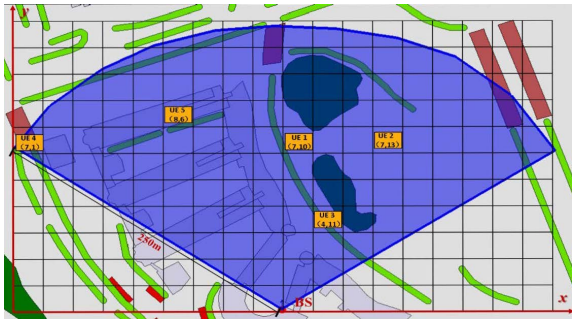

Fig. 2. Illustration of channel measurement campaign scenarios in Ray-tracing dataset.

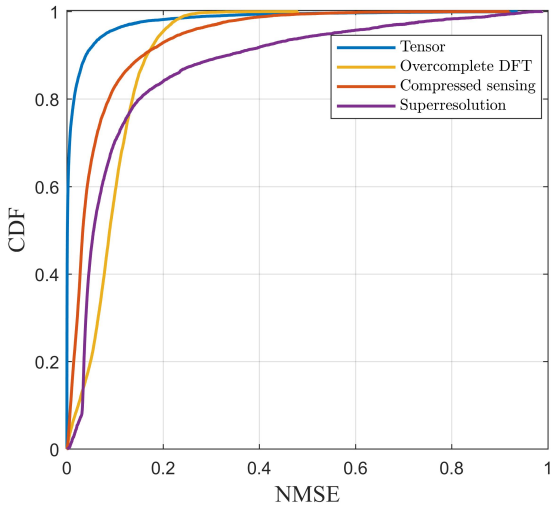

Fig. 3. CDF comparison of downlink channel reconstruction in Ray-tracing dataset.

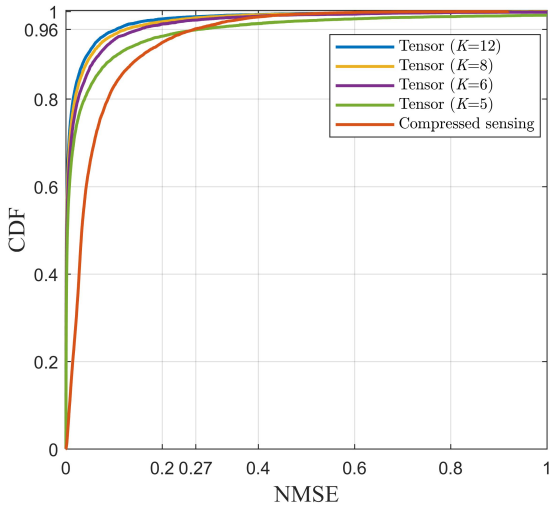

Fig. 4. CDF comparison of downlink channel reconstruction with different number of pilot symbols in Ray-tracing dataset.

highest energy bases are determined from the uplink channel, and their coefficients used for downlink channel reconstruction are refined in the downlink training stage. The sampling grid points for the DFT basis in the horizontal angle, vertical angle, and frequency domains are all set to 64, which means that the oversampling rate of the grid points is 4. For fairness, we also set the oversampling rate of the grid points to 4 for the compressed sensing method.

As shown in Fig. 3, the proposed tensor-based method achieves the best reconstruction performance, which demonstrates its superior accuracy in channel parameter estimation than other methods. The compressed sensing method yields the second best NMSE result on the average. However, its performance is highly dependent on the predefined grid points in the angular and the delay domains, and thus may degrade when the actual angle and delay parameters are not on the grids that we set. An analogous phenomenon of angle and delay mismatch occurs in the overcomplete DFT method, resulting in the energy leakage in the DFT basis. It is observed that the superresolution method does not perform well in the Ray-tracing dataset. The reason is that the channel data in this dataset do not meet the minimum separation condition for the delay parameter superresolution, which is related to the number of paths L, number of subcarriers N, and the subcarrier spacing Δf [19].

Next, we evaluate the effectiveness of the proposed downlink pilot transmission scheme in the downlink gain estimation stage. We follow the above experimental settings, but reduce the pilot overhead by transmitting fewer OFDM symbols than the number of antennas at the BS, i.e., $K < M$. Then, the downlink gain parameters of the multipath components are estimated by (21) and used for downlink channel reconstruction. Fig. 4 plots the CDF curve of the proposed tensor-based method in different cases of K. Regarding the CDF curve of the compressed sensing method as the baseline, we see that the proposed tensor-based method obtains better reconstruction results even when only 6 OFDM symbols are transmitted for downlink training. In the more challenging case of $K = 5$, the tensor-based and compressed sensing methods yield an intersection on the CDF curves at about NMSE=0.27, which implies that the tensor-based method performs better on an average of 96% of UE scenarios in the dataset.

V. Conclusion

In this paper, we have proposed a tensor-based method to reconstruct the downlink channel in FDD massive MIMO systems. In the proposed method, the dual-polarized MIMO channel is modeled as a forth-order tensor, whose CP decomposition is used to estimate the angle and delay parameters from the uplink channel. After estimating the downlink gain parameters through training and feedback, we have employed the partial reciprocity in the FDD mode to reconstruct the downlink channel from the estimated angle, delay and gain parameters. The downlink channel reconstruction results with a Ray-tracing dataset show that the proposed tensor-based method outperforms the overcomplete DFT, compressed sensing and superresolution methods in terms of reconstruction accuracy.

References

[1] Z. Zhong, L. Fan and S. Ge, "FDD massive MIMO uplink and downlink channel reciprocity properties: Full or partial reciprocity?" in *Proc. IEEE Global Commun. Conf.*, 2020, pp. 1–5.

[2] P. Zhao, Z. Wang and C. Sun, "Angular domain pilot design and channel estimation for FDD massive MIMO networks," in *Proc. IEEE Int. Conf. Commun.*, 2017, pp. 1–6.

[3] Y. Han, T. Hsu, C. Wen, K. Wong, and S. Jin, "Efficient downlink channel reconstruction for FDD multi-antenna systems," *IEEE Trans. Wireless Commun.*, vol. 18, no. 6, pp. 3161–3176, 2019.

[4] Y. Han, Q. Liu, C. Wen, M. Matthaiou, and X. Ma, "Tracking FDD massive mimo downlink channels by exploiting delay and angular reciprocity," *IEEE J. Sel. Topics Signal Process.*, vol. 13, no. 5, pp. 1062–1076, 2019.
[5] H. Xie, F. Gao, S. Jin, J. Fang, and Y.-C. Liang, "Channel estimation for TDD/FDD massive MIMO systems with channel covariance computing," *IEEE Trans. Wireless Commun.*, vol. 17, no. 6, pp. 4206–4218, 2018.
[6] J. Dai, A. Liu and V. K. N. Lau, "FDD massive MIMO channel estimation with arbitrary 2D-array geometry," *IEEE Trans. Signal Process.*, vol. 10, no. 15, pp. 2584–2599, 2018.
[7] N. Garg, M. Sellathurai and T. Ratnarajah, "Low complexity joint OMP methods for FDD channel estimation in Massive MIMO systems," in *Proc. 21th IEEE Workshop Signal Process. Adv. Wireless Commun.*, 2020, pp. 1–5.
[8] W. Yang, L. Chen and Y. E. Liu, "Super-resolution for achieving frequency division duplex (FDD) channel reciprocity," in *Proc. 19th IEEE Workshop Signal Process. Adv. Wireless Commun.*, 2018, pp. 1–5.
[9] Y. Liu and X. Jiang, "Robust super-resolution frequency division duplex (FDD) channel estimation," in *Proc. IEEE 11th Sens. Array Multichannel Signal Process. Workshop,* 2020, 1–5.
[10] B. Mamandipoor, D. Ramasamy and U. Madhow, "Newtonized orthogonal matching pursuit: Frequency estimation over the continuum," *IEEE Trans. Signal Process.*, vol. 64, no. 19, pp. 5066–5081, 2016.
[11] N. D. Sidiropoulos, L. De Lathauwer, X. Fu, K. Huang, E. E. Papalexakis, and C. Faloutsos, "Tensor decomposition for signal processing and machine learning," *IEEE Trans. Signal Process.*, vol. 65, no. 13, pp. 3551–3582, 2017.
[12] G. J. Foschini and M. J. Gans, "On limits of wireless communications in a fading environment when using multiple antennas," *Wireless Pers. Commun.*, vol. 6, no. 3, pp. 311–335, 1998.
[13] C. Qian, X. Fu, N. D. Sidiropoulos, and Y. Yang, "Tensor-based channel estimation for dual-polarized massive MIMO systems," *IEEE Trans. Signal Process.*, vol. 66, no. 24, pp. 6390–6403, 2018.
[14] T. G. Kolda, "Multilinear operators for higher-order decompositions," Tech. Rep. SAND2006-2081, Sandia Nat. Laboratories, 2006.
[15] F. Roemer and M. Haardt, "Tensor-based channel estimation and iterative refinements for two-way relaying with multiple antennas and spatial reuse," *IEEE Trans. Signal Process.*, vol. 58, no. 11, pp. 5720–5735, 2010.
[16] B. D. Rao and K. S. Hari, "Performance analysis of root-music," *IEEE Trans. Acoust., Speech, Signal Process.*, vol. 37, no. 12, pp. 1939–1949, 1989.
[17] C. Qian, L. Huang, H.-C. So, N. D. Sidiropoulos, and J. Xie, "Unitary PUMA algorithm for estimating the frequency of a complex sinusoid," *IEEE Trans. Signal Process.*, vol. 63, no. 20, pp. 5358–5368, 2015.
[18] Z. Zhou, J. Fang, L. Yang, H. Li, Z. Chen, and S. Li, "Channel estimation for millimeter-wave multiuser MIMO systems via PARAFAC decomposition," *IEEE Trans. Wireless Commun.*, vol. 15, no. 11, pp. 7501–7516, 2016.
[19] E. J. Candès and C. F.-Granda, "Towards a mathematical theory of super-resolution," *Comm. Pure Appl. Math*, vol. 67, no. 6, pp. 906–956, 2014.